REPORT DOCUMENTATION

AFRL-SR-BL-TR-98-

0557

oved
0704-0188

1. AGENCY USE ONLY (Leave blank)	2. REPORT DATE	3. REPORT TYPE AND DATES COVERED
	January 1998	Technical, 9/96 - 12/97 (FINAL)

4. TITLE AND SUBTITLE

Fracture Phenomena and Interface properties of Composites: A Fundamental Approach

5. FUNDING NUMBERS

F49620-96-1-0467

6. AUTHOR(S)

Arif Masud and John Botsis

7. PERFORMING ORGANIZATION NAME(S) AND ADDRESS(ES)

Dept. of Civil and Materials Engineering
University of Illinois at Chicago
842 West Taylor Street
Chicago, IL 60607

8. PERFORMING ORGANIZATION REPORT NUMBER

9. SPONSORING/MONITORING AGENCY NAME(S) AND ADDRESS(ES)

AFOSR
110 Duncan Avenue, Suite B115
Bolling AFB DC 20332-0001

10. SPONSORING/MONITORING AGENCY REPORT NUMBER

19980803 102

11. SUPPLEMENTARY NOTES

12a. DISTRIBUTION/AVAILABILITY STATEMENT

Approved for public release;
distribution unlimited.

12b. DISTRIBUTION CODE

13. ABSTRACT *(Maximum 200 words)*

This report presents a numerical approach to study the effects of bridging and shielding fibers on reduction in Stress Intensity Factor (SIF) at the crack tip. The variational foundation of the formulation is based on a modified Hu-Washizu variational principle. The crack is assumed to grow in a self-similar manner and an energy approach is undertaken to evaluate SIF at the crack tip. A perfect bond is assumed between the fiber and the matrix to account for the interaction of the two phases. It is observed that the area around the crack tip where the fibers strongly influence SIF extends to about three fibers ahead of the crack and five fibers in the wake of the crack. Numerical simulations also show that there is a certain limit beyond which increasing the ratio of the modulus of elasticity of the fibers w.r.t. the matrix may not help in reducing the SIF at the crack tip. A detailed study on the inter-phase stress fields around the reinforcing fibers shows that stronger fibers have a larger zone of influence and can potentially effect the stresses around the neighboring fibers. A study on temperature change indicates that thermal gradients result in a redistribution of the stress field and thus can have pronounced effect on the stress field at the crack tip.

14. SUBJECT TERMS

Discrete fiber-matrix system, finite elements, shielding effect, bridging effect, thermal effect

15. NUMBER OF PAGES

16. PRICE CODE

17. SECURITY CLASSIFICATION OF REPORT	18. SECURITY CLASSIFICATION OF THIS PAGE	19. SECURITY CLASSIFICATION OF ABSTRACT	20. LIMITATION OF ABSTRACT
Unclassified	Unclassified	Unclassified	UL

ABSTRACT

Fibrous and laminated composites have become an important class of materials that is increasingly being used in engineering structures. However, unlike the common engineering materials, characterizing the fracture behavior of fibrous composites is a difficult task. In this work we have adopted a numerical approach to study the effects of bridging and shielding fibers on reduction in Stress Intensity Factor (SIF) at the crack tip. This report presents a finite element formulation of elasticity to model elastic fracture in composites with long aligned fibers. We have employed $\bar{B}$-bar type approach which is applicable to compressible as well as nearly incompressible material systems. The variational foundation of the formulation is based on a modified Hu-Washizu variational principle. The crack is assumed to grow in a self-similar manner and an energy approach is undertaken to evaluate the stress intensity factor at the crack tip. A perfect bond is assumed between the fiber and the matrix to account for the interaction of the two phases. The effects of strong intact bridging fibers, fiber ahead of the crack tip, and that of temperature variation on the reduction in stress intensity factor at the crack tip have been investigated. Various numerical results are presented to show fiber-fiber and fiber-crack interaction.

SIGNIFICANT FINDINGS

We have adopted a novel computational approach to investigate the bridging and the shielding mechanism and their effect on the stress field at crack tip without any other dissipative mechanisms. The following main points can be drawn from the results of the present numerical studies.

1. The effect of the bridging fibers on SIF is much larger than that of the fibers ahead of the crack tip.

2. The area around the crack tip where the fibers strongly influence the stress intensity factor extends to about three fibers ahead of the crack and five fibers in the wake of the crack.

3. As for the effect of the modulus of elasticity of the fibers on SIF, the results indicate that for values greater than $E_f/E_m = 15$ the effect is relatively small. Making fibers too strong with respect to the matrix (beyond a certain limit) may not help in reducing the stress intensity factor at the crack tip.

4. We have also studied the inter-phase stress fields around the reinforcing fibers that show steep gradients normal to the interface. It is seen that stronger fibers have a larger zone of influence and can potentially effect the stresses around the neighboring fibers. The present study also confirms that homogenization of the composite system cannot predict the discrete stress distribution at crack tip and fiber-matrix interfaces, and thus can lead to erroneous conclusions.

5. The effects of temperature change have also been studied in the presence of a bridging fiber. These preliminary results indicate that thermal gradients can result in a redistribution of the stress field and thus can have pronounced effect on the stress field at the crack tip. It also shows the importance of a coupled thermo-mechanical theory for possible elasto-plastic yielding of the matrix material at the tip of the crack. Such elasto-plastic deformation would considerably alter the stress field in a localized zone in the viscinity of the crack.

TABLE OF CONTENTS

LIST OF FIGURES

1. Introduction

Composite materials, e.g., metal, ceramic and polymer reinforced with long aligned fibers have shown significant promise in the design of advanced aerospace systems. Their high strength to weight ratio and the flexibility to tailor make these materials with performance that is superior to their constituent materials are the main attributes. However, unlike the common engineering materials, the fracture behavior of composites has not been well understood. Thus, understanding strength and fracture behavior of these materials has been the subject of intense investigation in the past several years. Because of the fact that the microstructures of real, commercially available composite materials are very complex and often difficult to characterize, it has been difficult to reveal basic mechanisms as well as elementary events that lead to fracture and failure in these advanced material systems. As a result, the lack of a rigorous failure criteria in composites made of advanced fibrous materials has ebbed away the confidence in using these materials in critical applications. Furthermore, it has resulted in high material qualification costs and overdesign weight penalties.

Mechanistic investigations have shown that several processes accompany fracture of composites. From a physical view point, some of them are related to micromechanics, while others to macromechanics, thus involving a wide range of scales. A complete characterization in space and time of these processes has often been a formidable experimental task. From an analytical viewpoint it is a non-smooth problem, involving various controlling parameters with associated spatial and temporal scales.

Among the various mechanisms with a significant contribution to fracture resistance of composites, crack bridging by intact fibers is considered to be very important. This is demonstrated by the large number of research works that have been

reported in the literature. Most of these works are dedicated to deriving analytical expressions for the stresses at the crack tip or toughness for cracks that exhibit steady or non-steady growth. However, experimental studies to attest these models have not received the same level of attention. This is perhaps due to the highly complex interactions between the various events and the difficulty to isolate their interactions.

Another mechanism that is also important in the increased fracture resistance of composites is an interaction of the crack and the fibers ahead of the crack. Studies on the interaction effects have also been reported albeit to a lesser extent. The essentially three dimensional problem that ensues renders an analytical solution very difficult. Thus simplifying assumptions are adopted for particular cases [1,2]. A more common approach has been to study the interaction between a crack and inclusion [3] or crack near or on a bi-material interface [4 - 6] using two dimensional configurations to derive solutions for the stress and strain fields as well as for the stress intensity factors. These solutions offer valuable insights in the interaction effects but their applicability to a fibrous composite system may be limited due to various length scales involved in the vicinity of a crack tip (Fig. 1).

To investigate some of the effects of fiber spacing and fiber type on strength and fracture, Botsis and co-workers [7 - 10] carried out research on composites with controlled fiber spacing. The results of these studies have shown that strength and fracture correlate well with fiber spacing. This approach offers certain advantages. By controlling the fiber architecture, the properties of the constituent materials and the interface, different types of behaviours can be simulated experimentally. Thus some of the pertinent parameters (fiber size, spacing, interface, etc.,) affecting strength, crack growth and debond evolution can be identified and thoroughly characterized. Results from such studies can be an important supplement to efforts

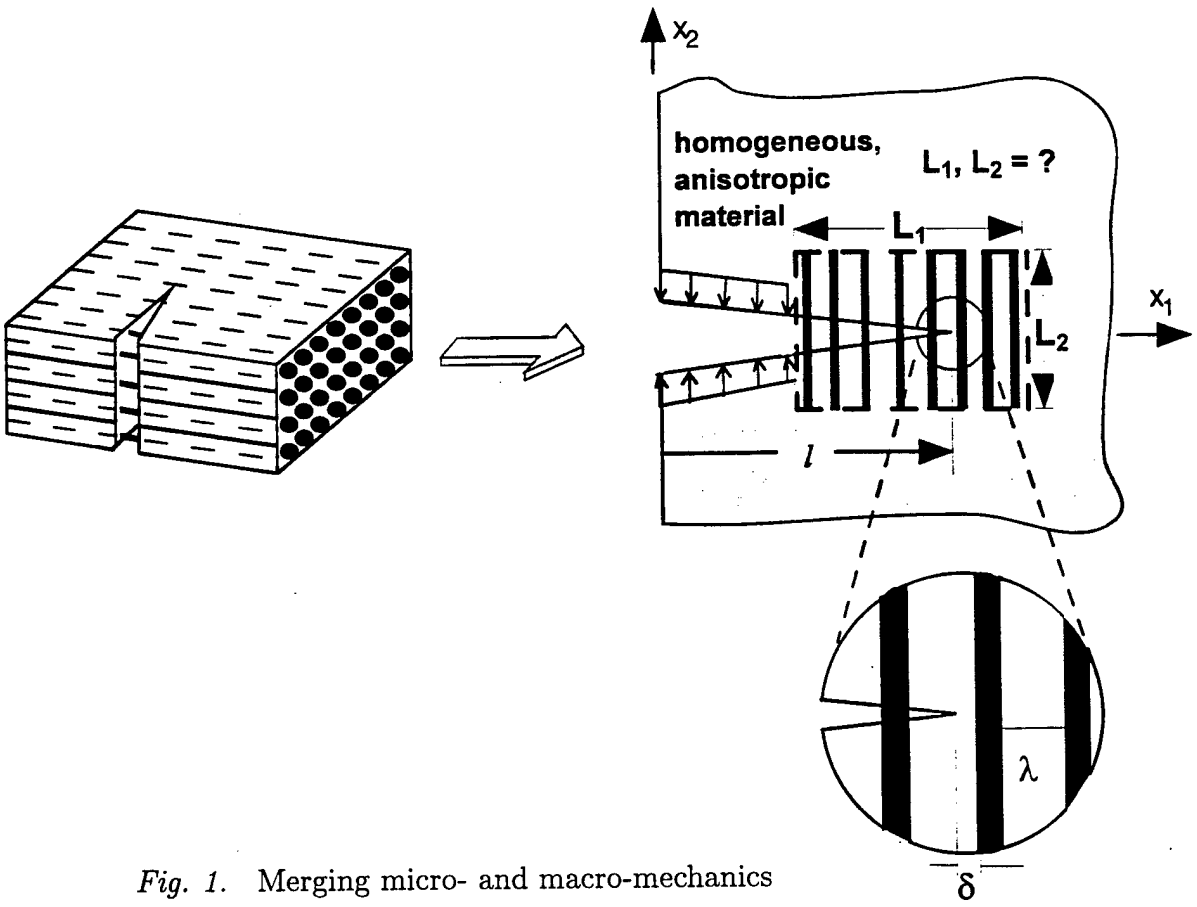

Fig. 1. Merging micro- and macro-mechanics

aimed at characterizing the response of composites particularly when a continuum approximation of the reinforcement is not realistic (Fig. 1). Such cases may arise when studying: (a) crack initiation, (b) driving forces of relatively short cracks, (c) the area around the tip of a long crack, (d) criteria for fracture, etc. Moreover, fiber spacing reflects the structure of the composite and is an intermediate scale since it is larger than the scales involved in fiber debonding, fracture and pull out. It is smaller, however, than the macro scales that arise in macrocracking and damage zones. Using this intermediate length scale within a continuum mechanics framework, a set of constitutive equations can be developed that incorporate this parameter which reflects the reinforcement better than volume average parameters.

The present work is aimed at investigating the effects of bridging fibers and fibers

in the path of the crack on the stress field and stress intensity factor. Emphasis is placed on a detailed stress analysis within a zone around the crack tip in an effort to establish its boundaries. (see Fig. 1). Outside this zone homogenization theories may be employed that consider the composite as an orthotropic material. At the boundary of this zone, appropriate conditions need to be imposed to consistently "glue" the two domains. Emphasis in this report is primarily numerical and rather practical in nature. We incorporate the inherent inhomogeneity and anisotropy in our framework at the variational level and look at material mismatch, interphase boundaries, interaction of the interface boundaries with each other and also with high stresses at the crack tip. These aforementioned issues render the ensuing problem 'non-smooth' in the classical sense and necessitate the solution method to be numerical in nature and founded on sound mathematical footings. We have employed the finite element method because it is based on variational principles and is a powerful numerical technique that offers a unified approach to such multiphase problems.

The report is divided into three main sections as follows: Section 2 presents the variational form of the problem. Section 3 develops the finite element formulation of the proposed model. Section 4 gives an account of the evaluation of the stress intensity factor. A detailed set of numerical simulations employing a carefully designed fiber architecture to uniaxial tension is presented in Section 5.

2. The Variational Framework

The insitu strength of a fibrous composite is not only a function of the properties of each of its constituent materials, it also depends on the various energy dissipation mechanisms that lead to matrix cracking and/or inelastic deformations, fiber debonding, slipping, and their ultimate fracture. Some of these mechanisms such as elasto-plastic deformations, damage and cracking in the matrix and necking and fracture in the bridging fibers can successfully be addressed at the constitutive level. However, fiber debonding and pull-out that leads to strong discontinuities in the displacement field is related to the interphase kinematics, and an appropriate way to handle them is to incorporate them in the variational framework. Our objective here is to develop a variationally sound approach that can be used to derive an energy based criteria for crack propagation and arrest in fibrous composites in the presence of one or more of the above mentioned mechanisms. Furthermore, an energy based approach for crack propagation and arrest can readily be extended to the nonlinear regime of material and geometric response. A general framework for such problems is provided by the *Hu-Washizu variational principle* which considers displacements, strains and stresses as the independent field variables.

Let $\Omega \subset \mathcal{R}^{n_{sd}}$ be a bounded open set with piecewise smooth boundary Γ, $n_{sd} \geq 2$ denotes the number of spatial dimensions. Let Γ_I represent the fiber-matrix interface with $\boldsymbol{u}^f$ and $\boldsymbol{u}^m$ be the displacement fields at the interface of the fibers and the matrix. We can write an energy functional for the hybrid system as

$$\Pi(\boldsymbol{\varepsilon}, \boldsymbol{\sigma}, \boldsymbol{u}, \boldsymbol{\lambda}) := \frac{1}{2}\int_{\Omega} \boldsymbol{\varepsilon} : \boldsymbol{c} : \boldsymbol{\varepsilon}\, d\Omega + \int_{\Omega} \boldsymbol{\sigma} \cdot [\nabla^s \boldsymbol{u} - \boldsymbol{\varepsilon}]\, d\Omega + \int_{\Gamma_I} \boldsymbol{\lambda}(\boldsymbol{u}^m - \boldsymbol{u}^f) d\Gamma - \Pi_{\text{ext}}(\boldsymbol{u}) \tag{1}$$

where $\boldsymbol{u}$, $\boldsymbol{\sigma}$ and $\boldsymbol{\varepsilon}$ are the unknown displacement, stress and strain fields, respectively, and $\boldsymbol{\lambda}$ is a Lagrange multiplier. $\Pi_{\text{ext}}(\boldsymbol{u})$ represents the external work on the composite system. The first term in (1) is the stored energy function, the second

term is a Lagrange multiplier($\boldsymbol{\sigma}$) enforcement of the strain-displacement relations ($\boldsymbol{\varepsilon} = \nabla^s \boldsymbol{u}$), and the third term is a Lagrange multiplier enforcement of the continuity of displacement field at the fiber matrix interface and corresponds to the interface energy. The Lagrange multiplier $\boldsymbol{\lambda}$ can be interpreted as a force quantity required to prevent relative displacement at the interface boundary. In the present work, we assume a perfect bond between the fiber and the matrix and thus preclude any debonding or pull out of fibers. Consequently the third term becomes identically zero leading to the following 3-field energy functional.

$$\Pi(\boldsymbol{\varepsilon}, \boldsymbol{\sigma}, \boldsymbol{u}) := \frac{1}{2}\int_\Omega \boldsymbol{\varepsilon} : \boldsymbol{c} : \boldsymbol{\varepsilon}\, d\Omega + \int_\Omega \boldsymbol{\sigma} \cdot [\nabla^s \boldsymbol{u} - \boldsymbol{\varepsilon}]\, d\Omega - \Pi_{\text{ext}}(\boldsymbol{u}) \tag{2}$$

We also want to develop a general framework that can encompass the compressible as well as slightly compressible or nearly- incompressible material systems. For example, metal matrix composites normally show a compressible elastic and isochoric (volume preserving) inelastic response while polymer based composites show a volume preserving or incompressible behavior even at small strains. It is well known that Galerkin approximation to incompressible or nearly-incompressible elasticity leads to eroneous results (Hughes [11]),e.g., mesh locking phenomenon, pressure oscillations, checker-board modes, to name a few. In the last two decades extensive research efforts have been directed to this issue and there are some well established techniques that can quite successfully handle the incompressible range of the response spectrum (Hughes [12, 13], Nagtegaal *et. al.* [14], Simo *et. al.* [15])

We assume the strain field to be divided into deviatoric and volumetric components

$$\begin{aligned} \boldsymbol{\varepsilon}(\boldsymbol{u}, \varphi) : &= \text{dev}\,[\nabla^s \boldsymbol{u}] + \frac{1}{n_{sd}}\varphi \mathbf{1} \\ &= \nabla^s \boldsymbol{u} + \frac{1}{n_{sd}}\,[\varphi - \text{div}\boldsymbol{u}]\,\mathbf{1} \end{aligned} \tag{3}$$

where $\boldsymbol{u} : \Omega \to \mathcal{R}^{n_{sd}}$ is the displacement field, $\varphi : \Omega \to \mathcal{R}$ is the spherical part of $\boldsymbol{\varepsilon}$ and is regarded as an *independent field*, and $\text{dev}[\cdot] := (\cdot) - \frac{1}{n_{sd}}\text{tr}(\cdot)\mathbf{1}$ represents

the deviatoric part of the indicated argument. The stress field which is compatible with the assumed strain field can be expressed as

$$\boldsymbol{\sigma}(\boldsymbol{u}, \varphi, p) = \text{dev}\,[\boldsymbol{D}\boldsymbol{\varepsilon}(\boldsymbol{u}, \varphi)] + p\mathbf{1} \tag{4}$$

where $\boldsymbol{D}$ represents the material constitutive matrix and p: $\Omega \rightarrow \mathcal{R}$ is an independent function which is to be interpreted as the hydrostatic pressure. By substituting (3) and (4) into the 3- field functional (2), we obtain the modified functional $\tilde{\Pi}(\boldsymbol{u}, \varphi, p)$

$$\tilde{\Pi}(\boldsymbol{u}, \varphi, p) = \frac{1}{2}\int_{\Omega} \boldsymbol{\varepsilon}(\boldsymbol{u}, \varphi) : \boldsymbol{c} : \boldsymbol{\varepsilon}(\boldsymbol{u}, \varphi) d\Omega + \int_{\Omega} p(\text{div}\boldsymbol{u} - \varphi) d\Omega - \Pi_{\text{ext}}(\boldsymbol{u}) \tag{5}$$

We denote the variations in volumetric strain φ and pressure p by ψ and q, respectively, all of which are only required to be square integrable, i.e. $L_2(\Omega)$ over the domain. As no boundary conditions are applied on stresses or strains, the admissible spaces of solutions and corresponding spaces of variations coincide, i.e., $\mathcal{D} := \{\varphi | \varphi \in [L_2(\Omega)]\}$, and $\mathcal{P} := \{p | p \in [L_2(\Omega)]\}$.

The boundary of domain Ω, denoted by Γ, is assumed to be piecewise smooth. We further assume that Γ is decomposed into two non-overlapping subregions Γ_g and Γ_h, where Γ_g is the portion of the boundary with prescribed displacement field $\boldsymbol{g}$, and Γ_h is the portion of the boundary with prescribed tractions $\boldsymbol{h}$. The admissible spaces for the displacement field and its variations are

$$\mathcal{S} = \{\boldsymbol{u} \in H^1(\Omega),\, \boldsymbol{u} : \Omega \rightarrow \mathcal{R}^{n_{sd}}; \boldsymbol{u} = \boldsymbol{g} \text{ on } \Gamma_g\} \tag{6}$$

$$\mathcal{V} = \{\boldsymbol{\omega} \in H_0^1(\Omega),\, \boldsymbol{\omega} : \Omega \rightarrow \mathcal{R}^{n_{sd}}\} \tag{7}$$

where $\mathcal{S}$ is the space of trial displacements and $\mathcal{V}$ is the associated space of weighting functions, respectively. $H^1(\Omega)$ denotes the space of square-integrable functions along with their generalized derivatives defined over Ω, and $H_0^1(\Omega)$ is the subset of $H^1(\Omega)$ whose members satisfy zero essential boundary conditions.

The minimization problem consists of finding the stationary point of (5) and satisfying the prescribed boundary conditions which are assumed to take the form

$$\boldsymbol{u} = \boldsymbol{g} \quad \forall \boldsymbol{x} \in \Gamma_g \tag{8}$$

$$\boldsymbol{\sigma} \cdot \boldsymbol{n} = \boldsymbol{h} \quad \forall \boldsymbol{x} \in \Gamma_h \tag{9}$$

where $\boldsymbol{n}$ denotes the unit outward normal to boundary Γ.

The stationarity conditions associated with (5) yield the variational form of the problem. For the case of small strains and static loads, and assuming the fibrous composite to occupy a region Ω in $\mathcal{R}^{n_{sd}}$, the formal statement of the variational form may be expressed as: Given $\boldsymbol{f} : \Omega \longrightarrow \mathcal{R}^{n_{sd}}$, $\boldsymbol{g} : \Gamma_g \longrightarrow \mathcal{R}^{n_{sd}-1}$, $\boldsymbol{h} : \Gamma_h \longrightarrow \mathcal{R}^{n_{sd}-1}$, find $(\boldsymbol{u}, \varphi, p) \in \mathcal{S} \times \mathcal{D} \times \mathcal{P}$ such that for all $(\boldsymbol{\omega}, \psi, q) \in \mathcal{V} \times \mathcal{D} \times \mathcal{P}$

$$(\nabla^s \boldsymbol{\omega}, \mathrm{dev}[\boldsymbol{D\varepsilon}(\boldsymbol{u}, \varphi)] + p\mathbf{1}) = (\boldsymbol{\omega}, \boldsymbol{f}) + (\boldsymbol{\omega}, \boldsymbol{h})_\Gamma \quad \forall \boldsymbol{\omega} \in \mathcal{V} \tag{10}$$

$$(q, \mathrm{div}\boldsymbol{u} - \varphi) = 0 \qquad \forall q \in L^2(\Omega) \tag{11}$$

$$(\psi, -p + \frac{1}{3}\mathrm{tr}[\boldsymbol{D\varepsilon}(\boldsymbol{u}, \varphi)]) = 0 \qquad \forall \psi \in L^2(\Omega) \tag{12}$$

where $(\cdot, \cdot)$ denotes the $L_2(\Omega)$ inner product, and $(\cdot, \cdot)_\Gamma$ represents the $L_2(\Gamma)$ inner product.

3. Finite Element Framework.

We now introduce the finite-dimensional approximations for displacements, strains and stresses as $\mathcal{S}^h \subset \mathcal{S}$, $\mathcal{V}^h \subset \mathcal{V}$, $\mathcal{D}^h \subset \mathcal{D}$ and $\mathcal{P}^h \subset \mathcal{P}$, respectively. The discrete displacement field and its variation are continuous globally, while the discrete stress and strain fields are assumed to be discontinuous across element boundaries. As a result of this discontinuous approximations, the discrete versions of (11) and (12) can be written over domain of an individual element Ω^e as

$$(q^e, \mathrm{div}\boldsymbol{u}^e - \varphi^e)_{\Omega^e} = 0 \tag{13}$$

$$(\psi^e, -p^e + \frac{1}{3}\mathrm{tr}[\boldsymbol{D}\boldsymbol{\varepsilon}(\boldsymbol{u}, \varphi)])_{\Omega^e} = 0 \tag{14}$$

Consequently, the stress and strain fields can be eliminated at the element level, leading to a modified displacement type formulation. With this end, we design discrete projection operator for the strain and pressure fields

$$\varphi^h = \mathbf{P}^T(\boldsymbol{x})\boldsymbol{\alpha}^e \tag{15}$$

$$p^h = \mathbf{P}^T(\boldsymbol{x})\boldsymbol{\beta}^e \tag{16}$$

where $\mathbf{P}^T(\boldsymbol{x}) = \{\gamma_1(\boldsymbol{x}), \cdots, \gamma_{n_\epsilon}(\boldsymbol{x})\}$, is a set of n_ϵ prescribed functions and $\boldsymbol{\alpha}^e$, $\boldsymbol{\beta}^e \in \mathcal{R}^{n_\epsilon}$ are n_ϵ local element parameters corresponding to strains and stresses, respectively.

We define the discrete divergence operator as

$$\mathrm{div}\boldsymbol{u}^{\mathrm{e}} = \boldsymbol{b}^{\mathrm{e}^{\mathrm{T}}}\boldsymbol{d}^{\mathrm{e}} \tag{17}$$

where $\boldsymbol{b}^{e^T} = \mathbf{1}^T\boldsymbol{B}^e$, and $\boldsymbol{B}^e$ is the usual strain-displacement matrix composed of derivatives of shape functions.

We also define a mean operator over element domain as

$$\boldsymbol{H}^e := \int_{\Omega^e} \mathbf{P}(\boldsymbol{x})\mathbf{P}(\boldsymbol{x})^T d\Omega \tag{18}$$

and assume that $\boldsymbol{H}^e$ *is invertible* (this condition is ensured if the n_ϵ functions $\gamma_1, \cdots, \gamma_{n_\epsilon}$ in $\mathbf{P}(\boldsymbol{x})$ are independent). Since any $q^h \in \mathcal{P}^h$ is discontinuous across element boundaries, equation (13) implies

$$\varphi^e = \mathbf{P}^T(\boldsymbol{x})\boldsymbol{H}^{e^{-1}} \int_{\Omega^e} \mathbf{P}(\boldsymbol{x}) \operatorname{div}\boldsymbol{u}^e d\Omega \tag{19}$$

for $e = 1, 2, \cdots, n_{el}$. Inserting (17) into (19) we finally obtain

$$\varphi^e = \mathbf{P}^T(\boldsymbol{x})\boldsymbol{H}^{e^{-1}} \int_{\Omega^e} \mathbf{P}(\boldsymbol{x})\boldsymbol{b}^e d\Omega\, \boldsymbol{d}^e \tag{20}$$

Thus, the effect of the interpolations (15) and (16) is to define a *modified discrete divergence operator* by expression (20), and is expressed as $\varphi^e \equiv \overline{\operatorname{div}}\boldsymbol{u}^e$.

Similarly substituting interpolations (15) and (16) in (14), we obtain

$$p^e = \mathbf{P}^T(\boldsymbol{x})\boldsymbol{H}^{e^{-1}} \int_{\Omega^e} \mathbf{P}(\boldsymbol{x}) \frac{1}{3}\operatorname{tr}[\boldsymbol{D}\boldsymbol{\varepsilon}(\boldsymbol{u}^e, \varphi^e)] d\Omega \tag{21}$$

Also by inserting (20) into the definition of the assumed strain field (3), we obtain the corresponding discrete version. Now substituting the discrete version of the assumed strain field together with expressions (20)and (21) in equation (10), we get a displacement version of the discrete variational form. It thus leads to an algebraic system of equations where the primary variable is the displacment field alone.

4. Evaluation of Stress Intensity Factor

Let Π^{strain} be the strain energy in equation (2). We evaluate this strain energy for two configurations of the specimen, i.e., for two different crack lengths l_1, l_2 ($l_2 > l_1$). From the two crack lengths and the calculated strain energies, the energy release rate for mode I crack growth is calculated as

$$G = \frac{\Pi_2^{\text{strain}} - \Pi_1^{\text{strain}}}{l_2 - l_1} \tag{22}$$

where Π_1^{strain} and Π_2^{strain} are the calculated strain energies at crack lengths l_1 and l_2, respectively. Using linear elastic fracture mechanics, the stress intensity factor for mode I crack is then computed as

$$K = \sqrt{\frac{E}{1-\nu^2}G} \quad \text{(plane strain)} \tag{23}$$

$$K = \sqrt{EG} \quad \text{(plane stress)} \tag{24}$$

where E and ν are the Young's modulus and Poisson's ratio of the matrix respectively.

5. Numerical Examples

In this section, we present various numerical experiments on 2-D plane strain specimens with straight fibers aligned along the loading direction. We study the interaction between the stress field around the crack tip and the inter-phase stress field that exists at the fiber-matrix interface. As it was pointed out in the introduction, the rows of fibers are replaced by layers of effective material. Furthermore, these numerical siumlations also represent a through-the-thickness transverse crack in a thick multilayered composite. Figure 2 shows the specimen geometry with a transverse notch and reinforcing fibers. Invoking symmetry in the geometry and loading, and assuming the crack to grow in a self-similar fashion, we have discretized only half of the specimen. The height (H) of the discrete specimen is one-half that of its width, i.e., $H = W/2$. The crack length is one third the specimen width, $l = W/3$. All reinforcing layers have a constant diameter $d = l/30$. Figure 3 shows a typical finite element mesh with one fiber in the path of the crack. We have assumed a perfect bond between fiber and matrix in the present simulations. The ratio of Young's Modulus for the various fibers with respect to the matrix E_f/E_m is 5, 15, 25, and 35. The Poisson's ratio for the reinforcement and matrix is $\nu_f = \nu_m = 0.3$.

In our numerical simulations, we are controlling the fiber spacing in the transverse direction to investigate the inter-relation between the interaction of crack and reinforcement and crack bridging.

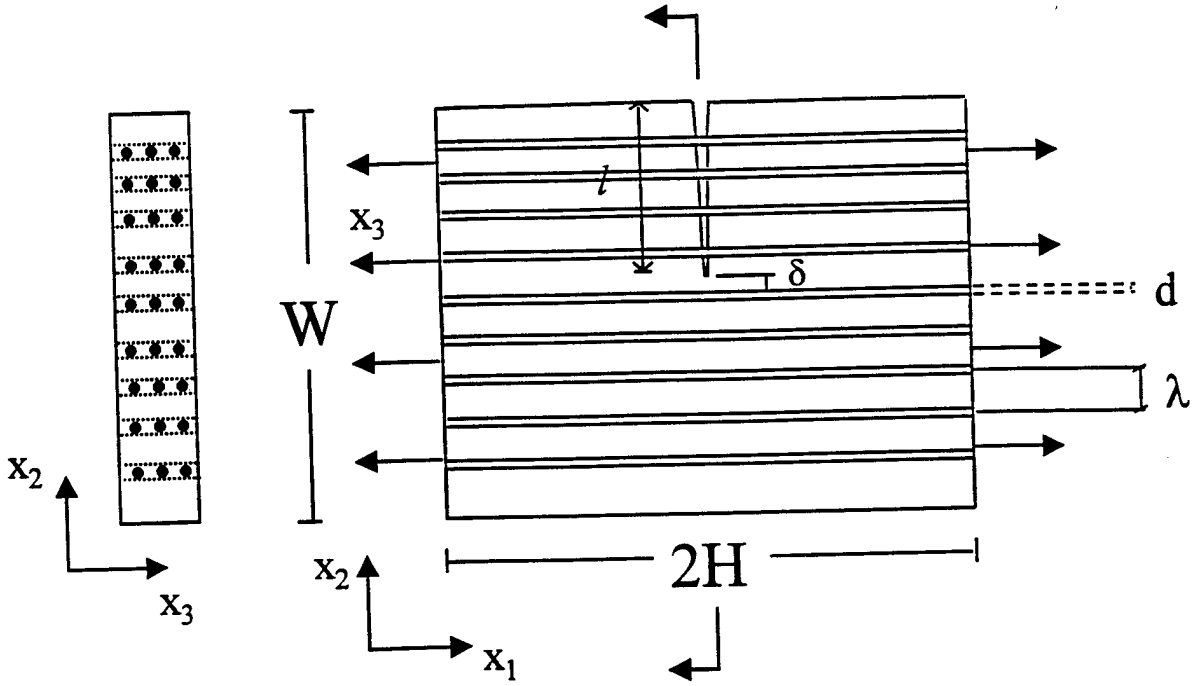

Fig. 2. Test specimen.

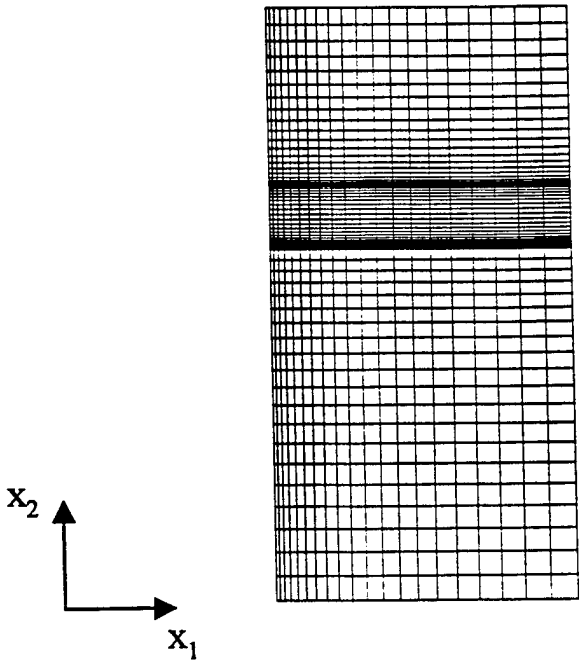

Fig. 3. Finite element mesh.

5.1 Shielding Effect: Proximity of fiber and reduction in SIF

Reinforcing fibers in the path of a crack play an important role in increasing the strength of a composite. This increase in strength is because of the interaction between the high stress at crack tip and the high stress gradients at fiber-matrix interface. This first test case investigates effect of proximity of a fiber ahead of the crack on the reduction in SIF. The specimen is loaded by applying 2% strain at the displacement boundary. In this test case we have considered only one layer of fibers that lie in the path of the crack. The distance δ between the reinforcement and the crack tip is varied (in multiples of the diameter of the fiber) between range $d \leq \delta \leq 10d$. The results are normalized with respect to the SIF obtained from homogeneous isotropic specimen subjected to same loading conditions. As can be seen in Fig. 4, bringing the fiber close to the crack reduces SIF at the crack tip. Furthermore, a stronger fiber results in a greater reduction in SIF as compared to a less stiff fiber because of the stiff inter-phase stress boundary. It is also worth noticing that after a distance of $10d$, the effect of the reinforcement on K_f has diminished considerably for all four cases of E_f/E_m.

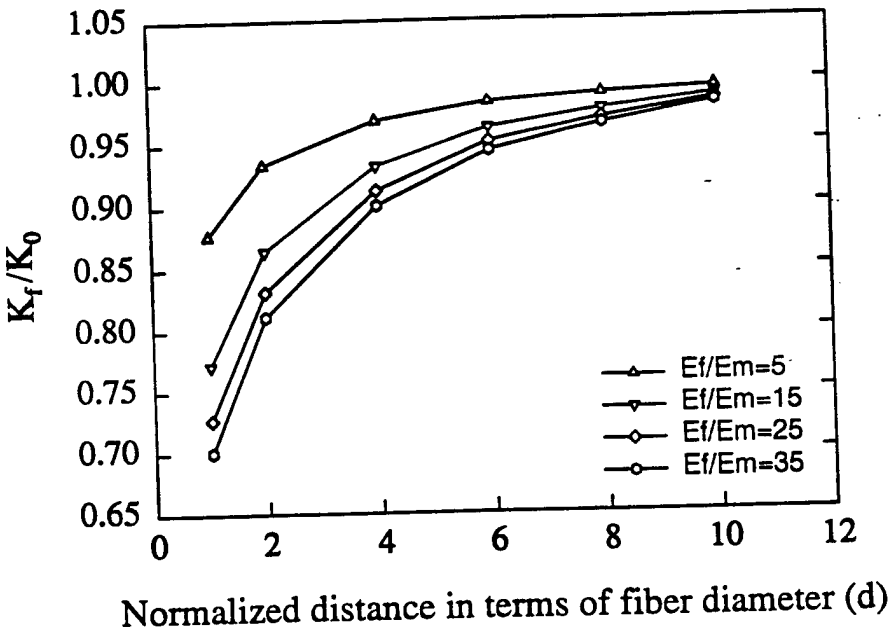

Fig. 4. Single fiber test. Effect of fiber proximity on reduction in K.

5.2 Effect of number of shielding fibers on reduction in SIF

This test case investigates the effect of number of fibers in the path of a crack on the reduction in SIF. The results of the simulations are shown in Fig. 5. The first reinforcing fiber is one diameter away from crack tip, i.e., $\delta = d$. The center-to-center distance between the subsequent fibers is 2d, i.e., $\lambda = 2d$. Normalization is performed with respect to the homogeneous isotropic specimen with crack of same dimension. The data in Fig. 5 shows that the first fiber has the greatest effect on K_f. The second fiber also has some effect but the third and fourth fibers have a considerably smaller influence on K_f. For the cases of $E_f/E_m = 5$ and 15 the third and fourth fiber have practically no effect. To examine any fiber-fiber interaction on the results of Fig. 5 we performed simulations of each fiber separately at their respective locations. The result of the simulations showed that, for the parameters of geometry and elastic constants, linear superposition can be used for the overall effect on K_f. To investigate the effect of E_f/E_m on K_f, the data in Fig. 5 are plotted as a function of E_f/E_m in Fig. 6. As seen in Fig. 6, the trend of the dependence is very similar and independent of the number of fibers. Apparently the first two fibers have the greatest effect on the total stress intensity factor. The addition of a third and fourth fibers have practically no effect.

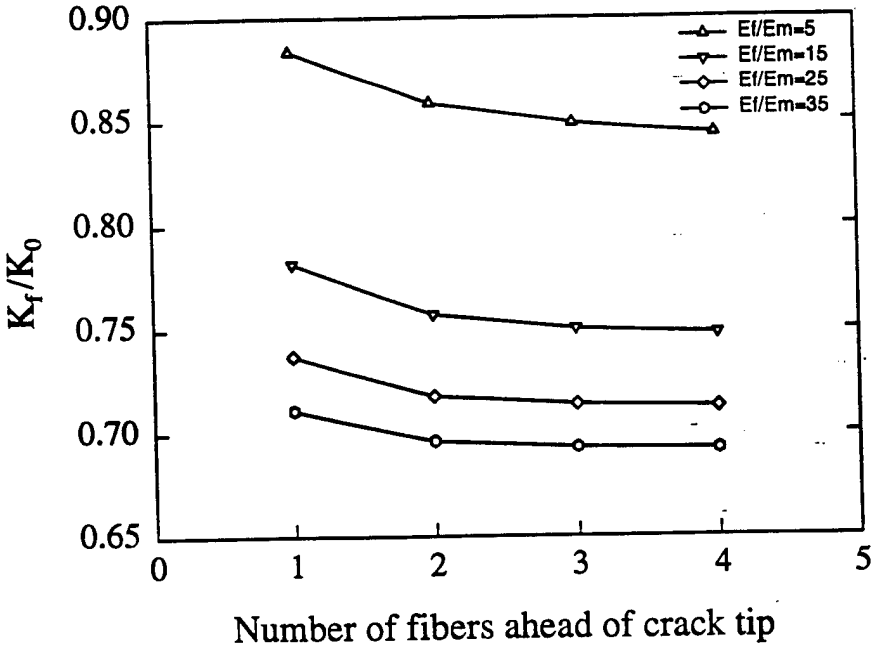

Fig. 5. Effect of number of fibers on reduction in K.

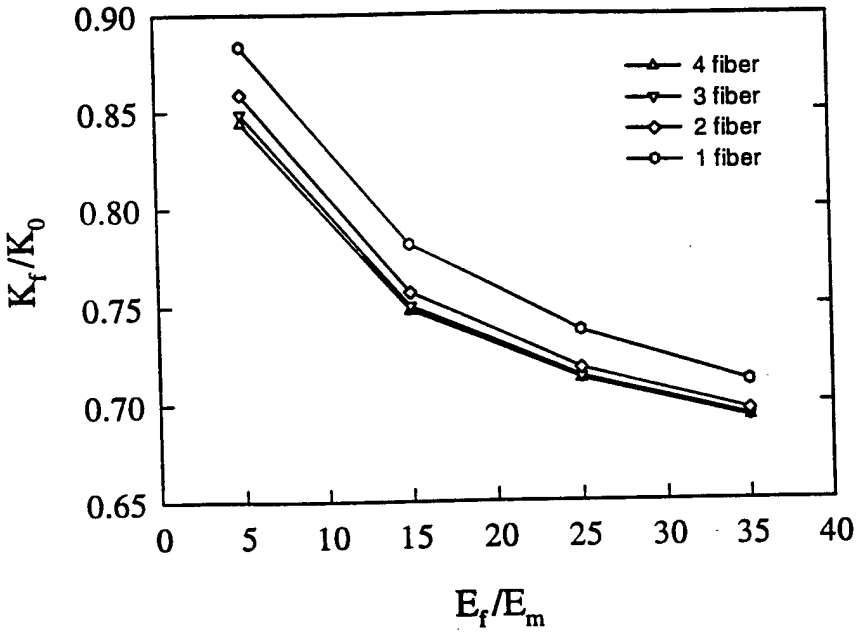

Fig. 6. Effect of E_f/E_m on K.

5.3 Spatial distribution of stress field

We first investigate the spatial distribution of σ_{11} in the path ahead of the crack. Figure 7-a shows the zoomed view of crack tip singularity in the homogeneous specimen. Here comparison is done with the analytical expressions. We know that unlike the analytical expression, numerical methods always give a finite value at crack tip. In the present case, the numerical method does capture the high gradient at crack tip. As our next step, we investigate the reduction in the intensity of stress at crack tip due to reinforcing fibers in the path of ahead of crack. Figure 7-b represents this reduction in crack tip stresses due to two shielding fibers. We can clearly see the drop in value by three folds. Furthermore, we can see the stress gradients across the width of the fibers as well. We have plotted a zoomed view of the region between crack tip and the fibers in Fig. 7-c which shows the steep stress gradients at the fiber matrix interfaces. We have also plotted $\ln(1/r)$ singularity along the two sides of adjacent fibers. Although we are not able to exactly catch the singularity, we certainly capture the extremely steep gradients in the stress field. This test case also validates the robustness of the formulation being used here for such "mathematically non-smooth" problems.

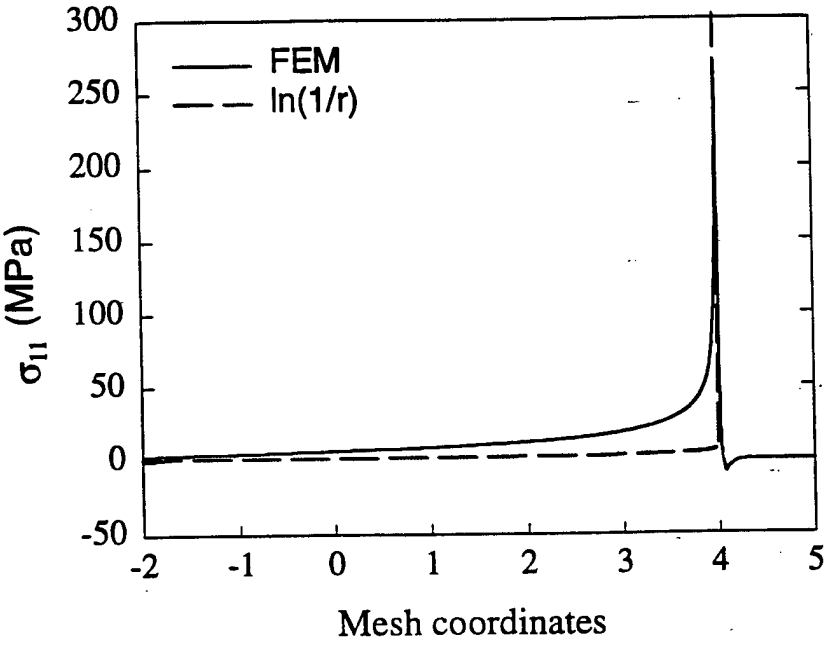

Fig. 7a. σ_{11} for homogeneous case.

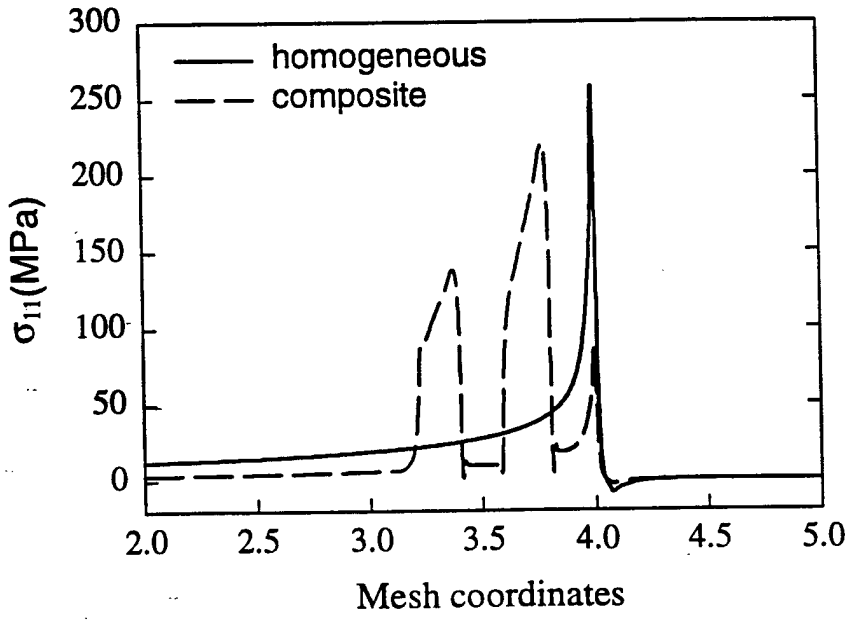

Fig. 7b. Crack-tip and fiber-matrix singularities.

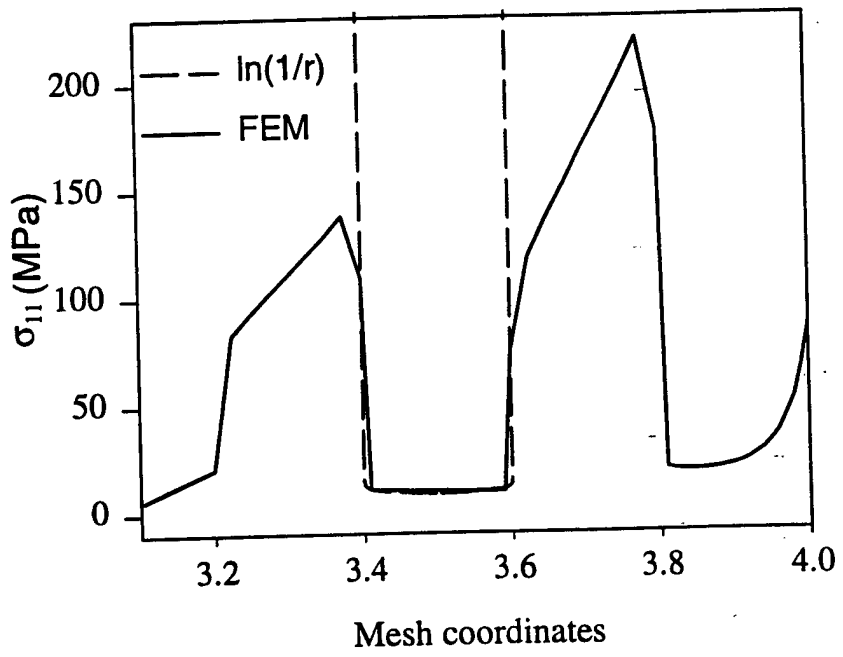

Fig. 7c. Zoomed view of fiber-matrix singularities.

To gain further insight on the stress distribution around the crack tip in the presence of the reinforcement we carried out two sets of simulations. In the first one we started with the specimen without reinforcement. Then we added a fiber at distance d from the crack tip and two more fibers at distances d from the first one and each other. We have not considered a fourth fiber because its effect on K_f was negligible (Fig. 5). We have loaded the specimen by applying 2% strain.

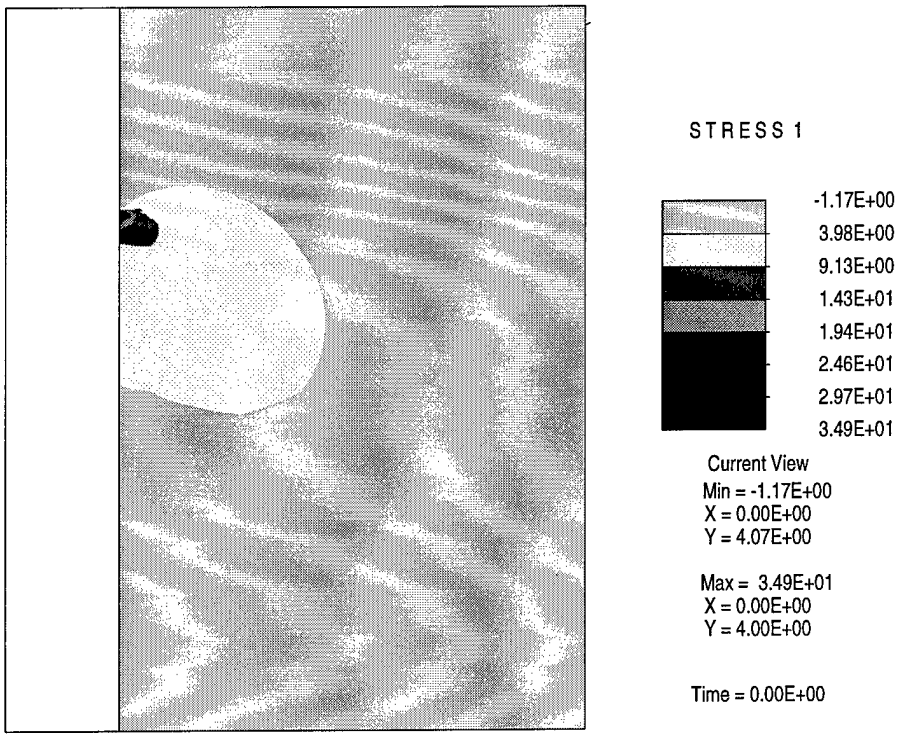

Fig. 8a. Effect of number of fibers on stress field - Homogeneous specimen.

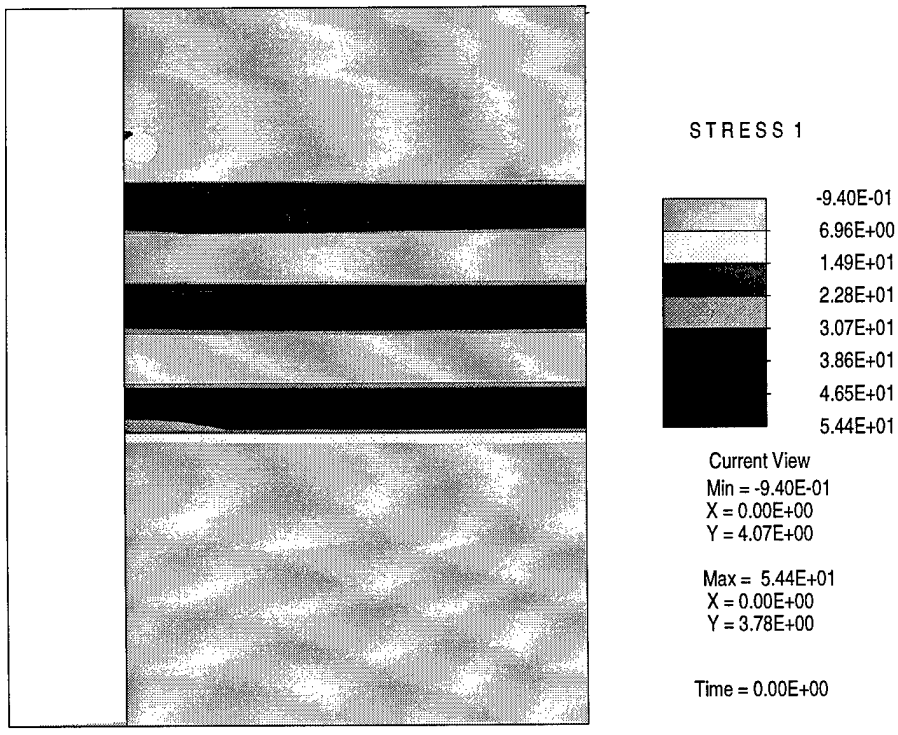

Fig. 8b. Effect of number of fibers on stress field - Fiber-matrix $E_f/E_m = 15$.

Figure 8 shows selective contours of the σ_{11} stress field, which are markedly different from that of the specimen without reinforcing fibers. We can also see the stress contours inside the fibers and extremely high stress gradients (sharp boundary layers) at the interface of the two materials. The iso-stress lines indicate that stress in the fibers at equal distances from the crack path depends on its proximity from the crack tip; the closest fiber being under the most stress. In this simulation E_f/E_m ratio is kept constant and equal to 15.

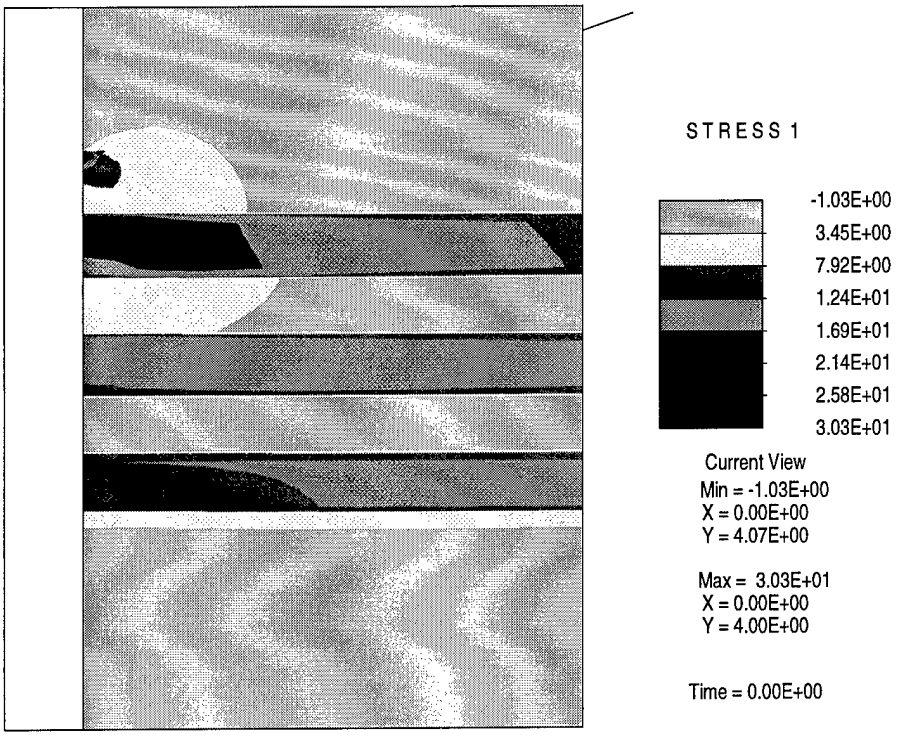

Fig. 9a. Effect of E_f/E_m on stress field - $E_f/E_m = 5$.

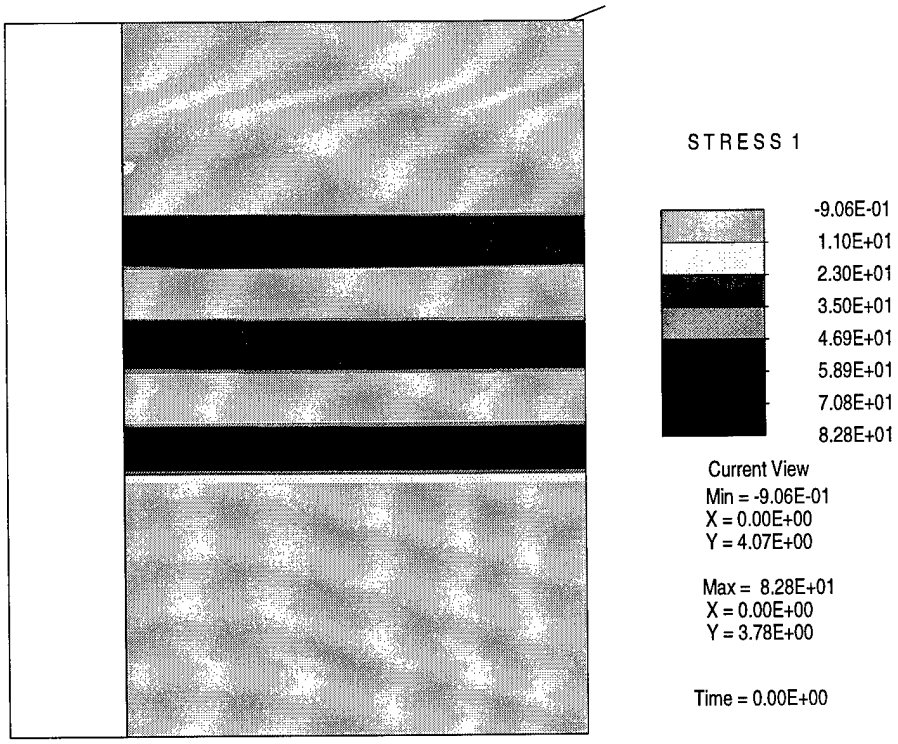

Fig. 9b. Effect of E_f/E_m on stress field - $E_f/E_m = 25$.

In the second simulation, we examined the effects of E_f/E_m on the stress fields σ_{11} around the crack tip in the presence of three fibers. Figure 9 presents the spatial stress distribution σ_{11} for E_f/E_m equal to 5 and 25, while keeping the number of fibers fixed equal to 3. As can be seen, the inter-phase stress boundary layers of stronger fibers e.g., Fig. 9-b have a larger zone of influence as compared to that of the weaker fibers, i.e., Fig. 9-a. Furthermore, interaction of the inter-phase stress boundaries can be seen in these figures.

5.4 Effect of a bridging fiber

In this numerical simulation we introduce an intact fiber in the bridging zone in addition to one reinforcing fiber in the path ahead of the crack tip (see Fig. 10). The motivation for this case study originates from the need to examine the relative effects of a bridging fiber and a fiber ahead of the crack tip on the stress intensity factor. To examine the contribution of a bridging fiber we vary the distance Δ between the fiber and the crack tip in terms of multiples of fiber diameter d with $d \leq \Delta \leq 6d$. A schematic of the fiber location is shown in Figure 10. The results of the simulations are shown in Fig. 11. Note that the reduction in normalized SIF is inversely proportional to fiber proximity in the wake of the crack. Normalization here is done with respect to homogeneous isotropic specimen with a crack of same dimension. Comparing Fig. 4 and Fig. 11 for E_f/E_m= 5 and $\delta = d$, we see that a fiber in the wake of crack reduces the normalized SIF to 3% of its values as compared to the one ahead of crack tip which reduces it down to approximately 87%. Consequently, for given E_f/E_m ratio and given δ from the crack tip, a bridging fiber is much more effective as compared to its counterpart ahead of the crack tip at the same distance.

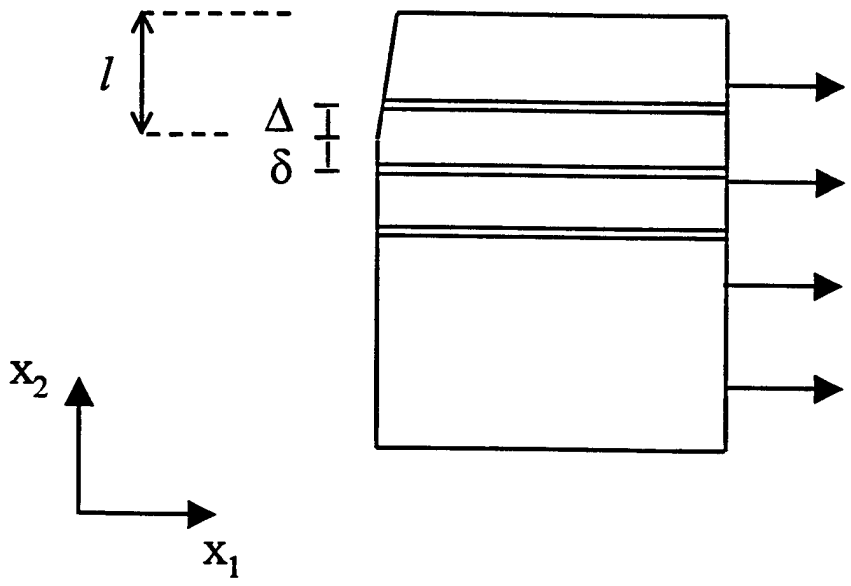

Fig. 10. Schematic diagram of the problem.

The normalized force in the bridging fiber (at the crack face) as a function of E_f/E_m ratio for various Δ values is plotted in Fig. 12. Here normalization in each case of Δ is done by dividing the force for various E_f/E_m ratios by their corresponding value of force for $E_f/E_m = 5$. It can be seen that for a given fiber crack-tip distance Δ, the stronger fibers carry more stress and shift the concentration of stress away from crack tip, thus resulting in considerable reduction in SIF.

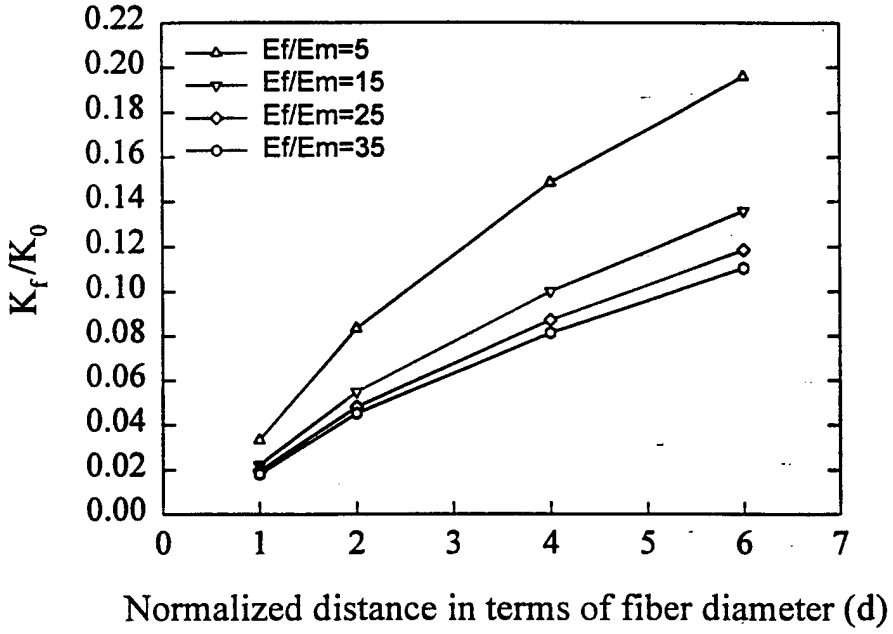

Fig. 11. Effect of bridging fiber proximity on reduction in K.

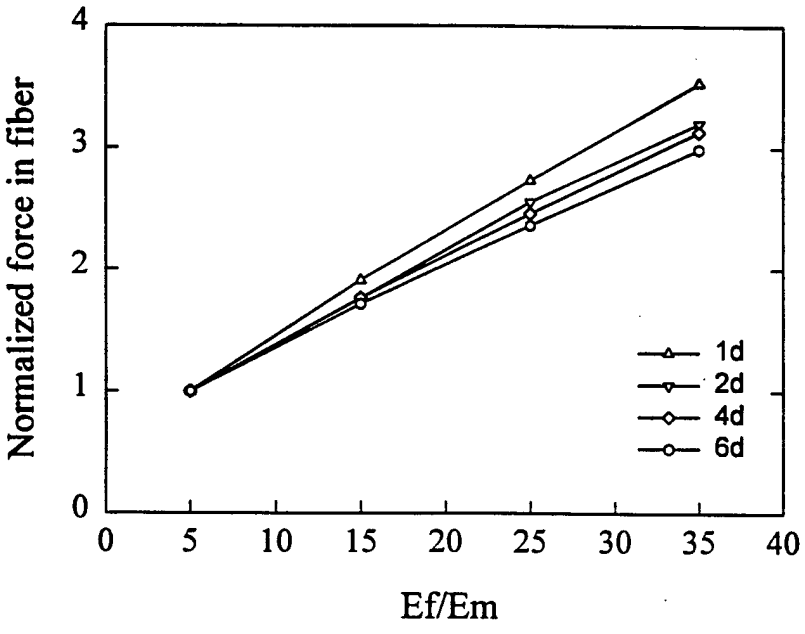

Fig. 12. Force vs. E_f/E_m in the bridging fiber.

5.5 Effects of the number of fibers in the bridging zone

To examine the reduction in SIF due to the number of fibers in the bridging zone and stress level along the crack path, we carried out simulations with three fibers ahead of the crack tip and adding one fiber at a time in the bridging zone. We have taken only three fibers along the crack path because the effects of additional fibers reduces the SIF insignificantly (Fig. 5). Loading is the same as in the previous tests. The distance of the first fiber, ahead of the crack tip is one diameter, i.e., $\delta = d$, and the surface-to-surface interfiber distance is two diameters, i.e., $\lambda = 2d$. The distance of the first bridging fiber from crack tip is $1d$, i.e., $\Delta = d$. The fibers in the bridging zone are added at distances of $2d$ (center-to-center).

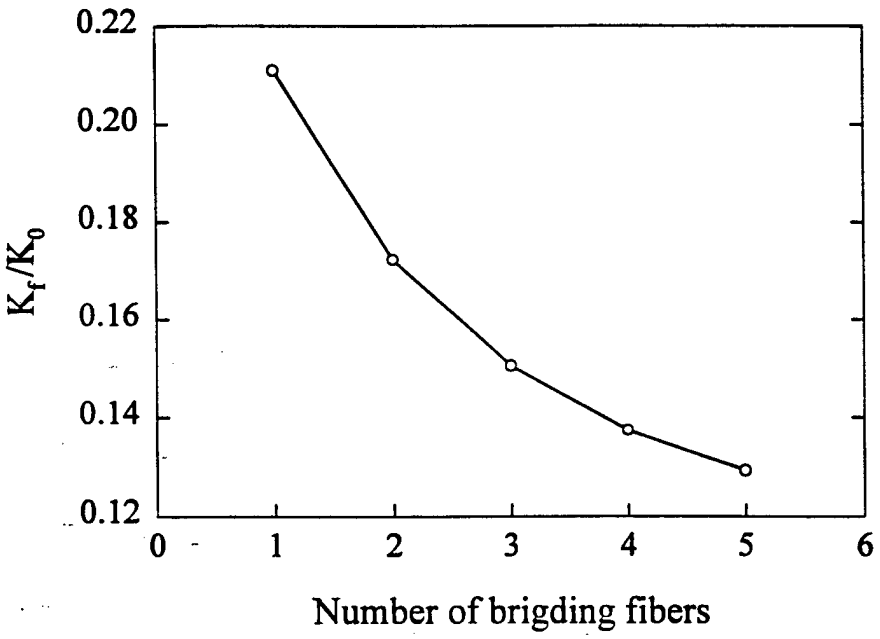

Fig. 13. Effect of number of bridging fibers on reduction in K.

Figure 13 shows the evolution of the normalized SIF as a function of the number of fibers in the bridging zone for the case when $E_f/E_m = 25$. The numerical data clearly demonstrates that the additional fibers further decrease the SIF at the

crack tip. However, the contribution of the first fibers is noticeably larger than that of other fibers. Moreover, the influence starts diminishing substantially after the fifth fiber. The effects of the ratio E_f/E_m on the SIF are displayed in Fig. 14. It is interesting to notice that the effects of E_f/E_m diminish rapidly and after $E_f/E_m = 15$ any further increase in E_f/E_m does not influence the SIF.

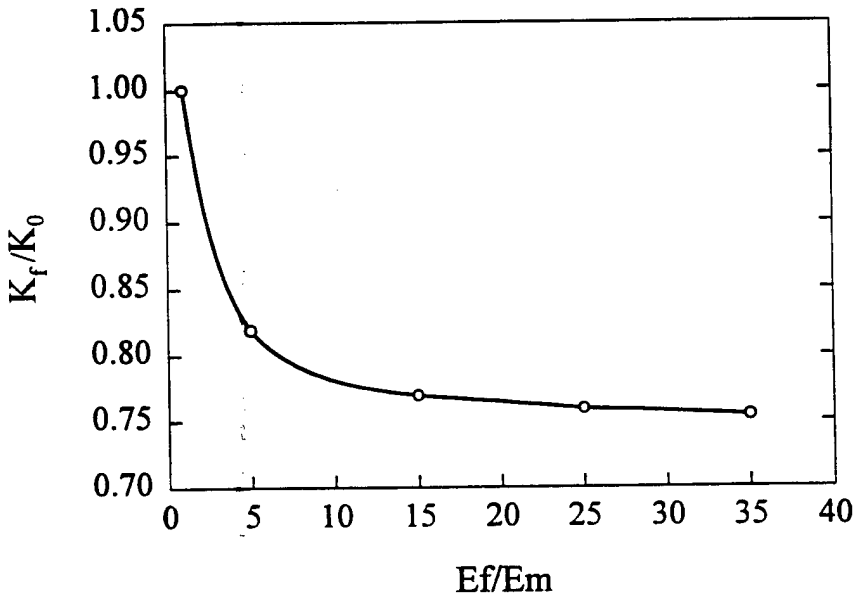

Fig. 14. Effect of relative strength of the fiber-matrix system on reduction in K.

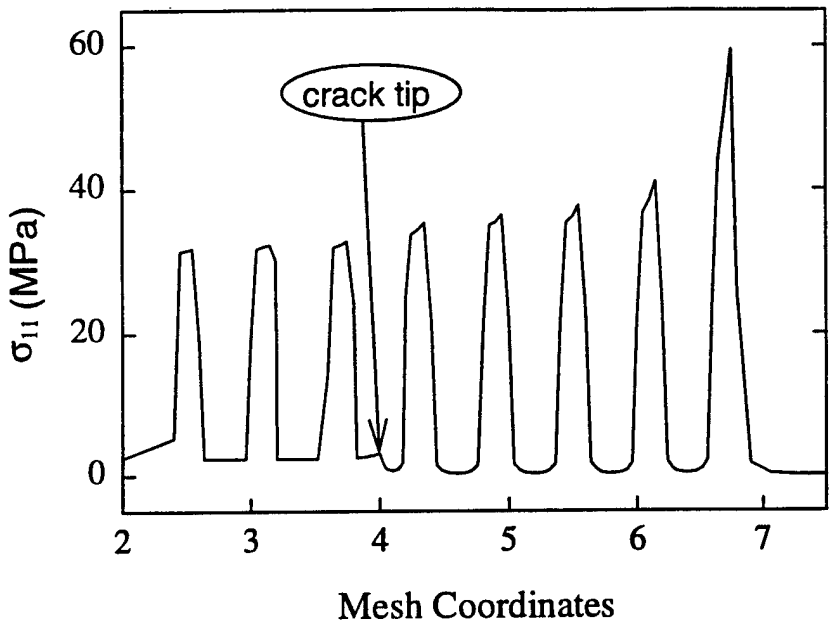

Fig. 15a. Stress distribution for fiber-matrix system - $E_f/E_m = 15$.

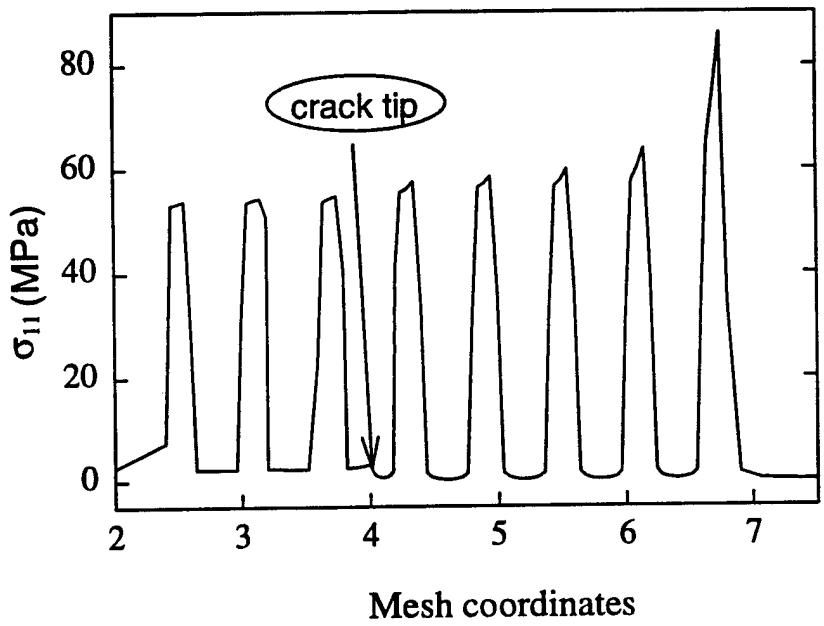

Fig. 15b. Stress distribution for fiber-matrix system - $E_f/E_m = 25$.

In this work we have also studied the normal stress (along line $x = 0$, see e.g. Fig. 10) ahead of the crack and in the bridging zone. The data of these simulations are shown in Fig. 15 for $E_f/E_m = 15$ (a) and $E_f/E_m = 25$ (b). Notice here that the stress in the fibers ahead of the crack tip is approximately the same in all three fibers, and about the same level as that given by the rule of mixtures. As for the stresses in the fibers in the bridging zone, there seems to be an small increase of the stress except for the fiber located the furthest from the crack tip. This fiber suffers the largest stress but contributes the least on the SIF.

Figure 16 shows the evolution of σ_{11} on the fibers in the bridging zone. It is interesting to notice that a cut-off length where the stress on the fibers equals that given by the rule of mixtures decays very quickly as we approach the crack tip. Furthermore, it can be seen that the computed stress field does not exhibit any spurious oscillations or checker board modes even under extremely high gradients. This simulation makes it precise that in order to study fibrous composites, the numerical method should be based on sound variational foundations because we inevitably have to use energy based criteria for crack propagation in these materials. Furthermore, it should also be able to capture the stresses as accurately as possible and should have the capacity to model steep gradients in stress fields.

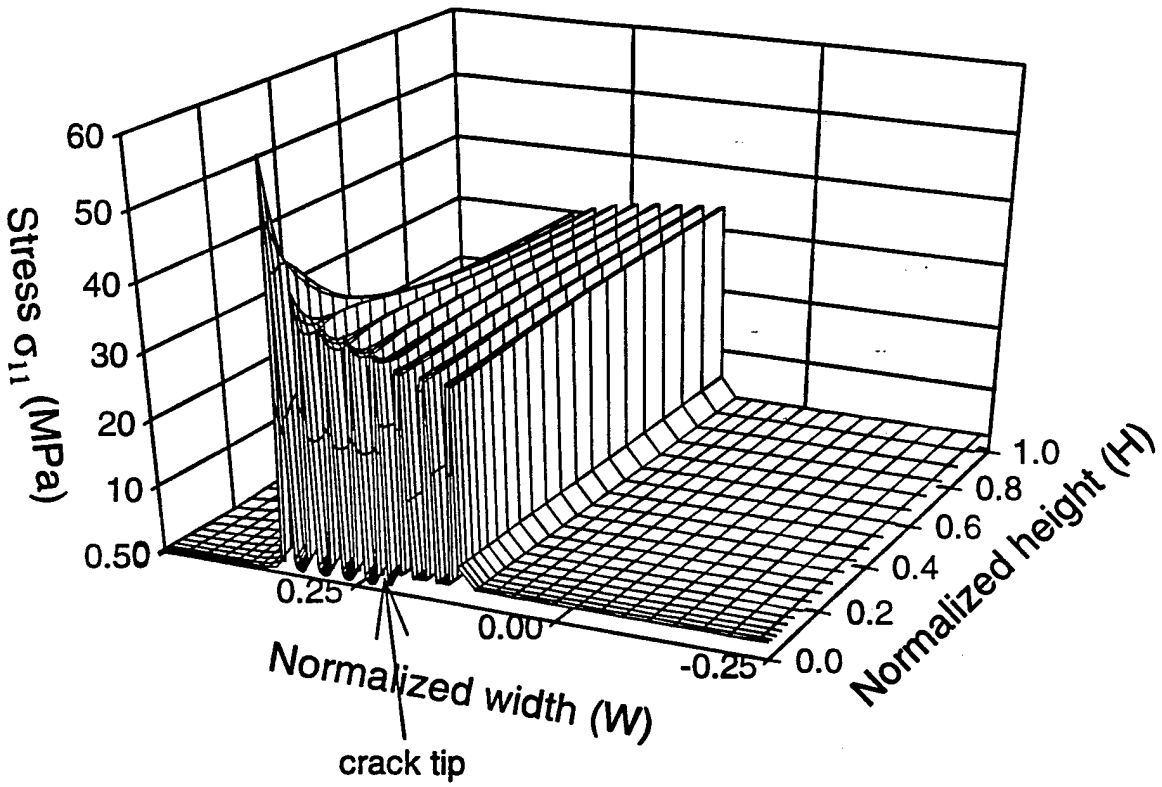

Fig. 16. 3-D projection of σ_{11} field.

5.6 Effect of uniform thermal stresses

Many practical applications of fibrous composites are under extreme thermal environments. Consequently, it seems appropriate to investigate the effects of thermal stresses on the stress field at crack tip in the matrix.

Temperature effects can be incorporated in the variational framework if the distribution of change in temperature $\Delta T(\boldsymbol{x})$ is known.

$$\Delta T(\boldsymbol{x}) = T(\boldsymbol{x}) - T_0(\boldsymbol{x})$$

where $T(\boldsymbol{x})$ is the current spatial distribution of temperature and $T_0(\boldsymbol{x})$ is the reference temperature distribution for zero thermal stresses in the composite. Let $\boldsymbol{\varepsilon}^{\text{th}}$ be the pointwise thermal gradient vector defined as

$$\boldsymbol{\varepsilon}^{\text{th}} = \kappa \langle \alpha_x \Delta T \quad \alpha_y \Delta T \quad 0 \rangle^T$$

where κ is 1 for plane stress and $(1+\nu)$ for plane strain. α_x and α_y are the coefficients of thermal expansion in x and y directions, respectively. Stresses are related to thermal strains via constitutive relation $\boldsymbol{\sigma} = \boldsymbol{c} : (\boldsymbol{\varepsilon} - \boldsymbol{\varepsilon}^{\text{th}})$. The effect of temperature can be accounted for at the variational level by replacing the first integral in equation (2) with a modified strain energy term written as

$$\begin{aligned} \Pi_{\text{strain}} &= \frac{1}{2} \int_\Omega \left(\boldsymbol{\varepsilon} - \boldsymbol{\varepsilon}^{\text{th}}\right) : \boldsymbol{c} : \left(\boldsymbol{\varepsilon} - \boldsymbol{\varepsilon}^{\text{th}}\right) \, d\Omega \\ &= \frac{1}{2} \int_\Omega \left[\left(\boldsymbol{\varepsilon} : \boldsymbol{c} : \boldsymbol{\varepsilon}\right) + \left(\boldsymbol{\varepsilon}^{\text{th}} : \boldsymbol{c} : \boldsymbol{\varepsilon}^{\text{th}}\right) - 2 \left(\boldsymbol{\varepsilon} : \boldsymbol{c} : \boldsymbol{\varepsilon}^{\text{th}}\right) \right] \, d\Omega \end{aligned} \tag{25}$$

where the first term in (25) is the usual strain energy and identical to the first integral in (2) while the remaining two terms incorporate the temperature effects.

The present simulation considers the thermal stresses that arise because of a change in the temperature of the fiber matrix system. In these simulations we load the specimen by applying a specified force at the boundary. The ratio of thermal coefficient for fiber and matrix $\alpha_f/\alpha_m = 10^{-1}$ and is assumed to be constant

over the range of temperature considered. The specimen consists of one bridging fiber at $\delta = 2d$ and no fibers in the path ahead of the crack. Figure 17 shows a linear reduction in SIF for various E_f/E_m ratios. We have also plotted the normalized force at the fiber tip (Fig. 18) where normalization is done with respect to zero temperature case. It can be observed that there is a corresponding linear increase in force in the fiber. This simulation points out that a variable coefficient of thermal expansion can play an important role in the analysis of bimaterial specimen. Consequently, a fully coupled thermo-mechanical theory that would evaluate the spatial distribution of thermal gradients and consequently effect the resultant stress field pointwise would be more appropriate for the analysis of fibrous composite systems.

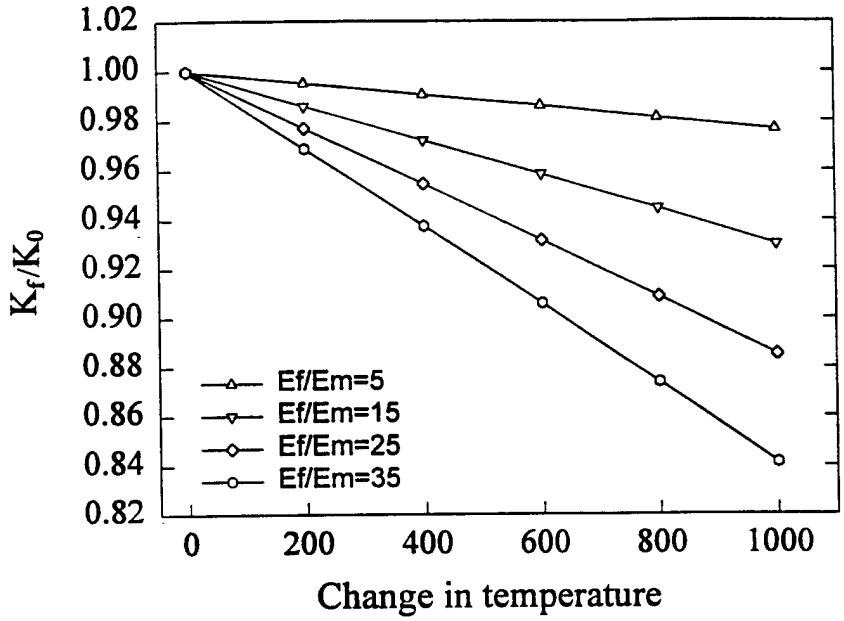

Fig. 17. Single fiber test. Effect of Temperature on K.

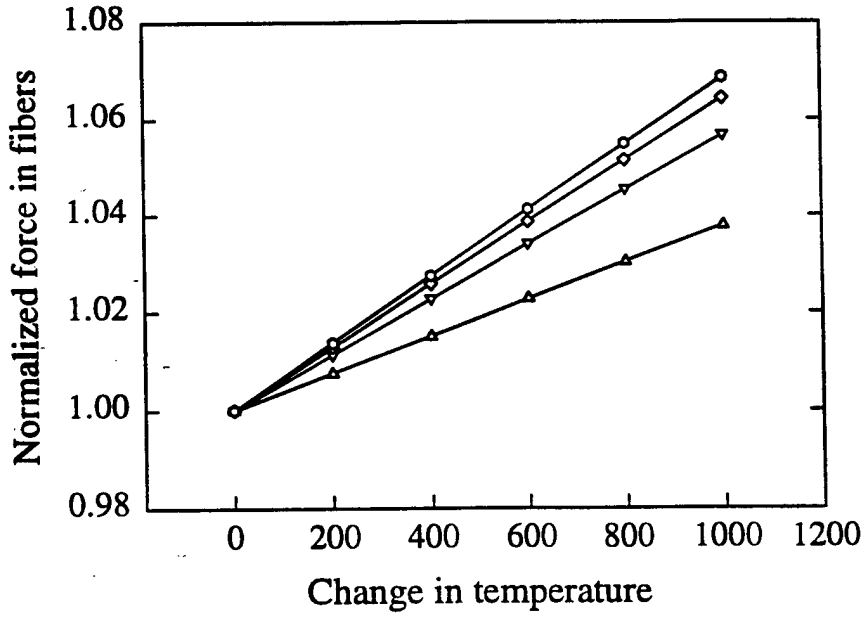

Fig. 18. Normalized reaction in the bridging fiber vs. temperature.

References

[1] H. Gao, J.R. Rice, "A first-order perturbation analysis of crack trapping by arrays of obstacles", *ASME Journal of Applied Mechanics*, **56**, 828, 1989

[2] A.F. Bower, M. Ortiz, "A three-dimensional analysis of crack trapping and bridging by tough particles", *Journal of the Mechanics and Physics of Solids*, **39**, 815, 1991

[3] A.A. Rubinstein, "Macrocrack-microdefect interaction', *ASME Journal of Applied Mechanics*, **53**, 505, 1986

[4] C. Atkinson, "On the stress Intensity Factors Associated with Cracks Interacting with an Interface Between wo Elastic Media", *International Journal opf Engineering Science*, **13**, 487-504, 1975

[5] F. Erdogan, G.D. Gupta and T.S. Cook, "Numerical solutions of Singular Intergral Equation", **1**, ed. G.C. Sih, Noordhoff International Publishing, 1053-1067, 1973

[6] A. Romeo, R. Ballarini, "A Crcack Very Close to a Bimaterial Interface", *ASMEJournal of Applied Mechanics*, **62**, 614 -619, 1995

[7] J. Botsis, C. Beldica and D. Zhao, *International Journal of Fracture*, **63**, 375, 1995

[8] D. Zhao, J. Botsis, "Experimental and Numerical Studies in Model composites Part I - Experimental Results", *International Journal of Fracture*, **82**, 153–174, 1996

[9] C. Beldica, J. Botsis, "Experimental and Numerical Studies in Model composites Part II - Numerical Results", *Journal of Fracture*, **82**, 175–192, 1996

[10] J. Botsis, D. Zhao, 'Fatigue Fracture Processes in a Model Composite', *Composites*, Part A, **28A**, 657-666, 1997

[11] T.J.R. Hughes, *The Finite Element Method: Linear Static and Dynamic Finite Element Analysis*, Prentice-Hall, Englewoods Cliffs, NJ, 1987.

[12] T.J.R. Hughes, "Generalization of selective integration procedures to anisotropic and nonlinear media", *International Journal for Numerical Methods in Engineering*, **15**, 1413–1418, 1980

[13] T.J.R. Hughes, "Recent developments in computer methods for structural analysis", *Nuclear Engineering and Design*, **57 No. 2**, 427–439, 1980

[14] J.C. Nagtegaal, D.M. Parks, and J.R. Rice, "On numerically accurate finite element", *Computer Methods in Applied Mechanics and Engineering* ,**4**, 153–178, 1974

[15] J.C. Simo, R.L. Taylor, and K.S. Pister, "Variational and projection methods for the volume constraint in finte deformation elasto-plasticty", *Computer Methods in Applied Mechanics and Engineering*, **51**, 177–208, 1985